Journal of Biomedical Optics

BiomedicalOptics.SPIEDigitalLibrary.org

Detection of canine skin and subcutaneous tumors by visible and near-infrared diffuse reflectance spectroscopy

Blaž Cugmas
Tanja Plavec
Maksimilijan Bregar
Peter Naglič
Franjo Pernuš
Boštjan Likar
Miran Bürmen

SPIE.

Detection of canine skin and subcutaneous tumors by visible and near-infrared diffuse reflectance spectroscopy

Blaž Cugmas,[a,b,*] Tanja Plavec,[c] Maksimilijan Bregar,[a] Peter Naglič,[a] Franjo Pernuš,[a,b] Boštjan Likar,[a,b] and Miran Bürmen[a,b]
[a]University of Ljubljana, Faculty of Electrical Engineering, Laboratory of Imaging Technologies, Tržaška 25, 1000 Ljubljana, Slovenia
[b]Sensum, Computer Vision Systems d.o.o., Tehnološki Park 21, 1000 Ljubljana, Slovenia
[c]University of Ljubljana, Veterinary Faculty, Clinic for Small Animal Medicine and Surgery, Gerbičeva 60, 1000 Ljubljana, Slovenia

Abstract. Cancer is the main cause of canine morbidity and mortality. The existing evaluation of tumors requires an experienced veterinarian and usually includes invasive procedures (e.g., fine-needle aspiration) that can be unpleasant for the dog and the owner. We investigate visible and near-infrared diffuse reflectance spectroscopy (DRS) as a noninvasive optical technique for evaluation and detection of canine skin and subcutaneous tumors *ex vivo* and *in vivo*. The optical properties of tumors and skin were calculated in a spectrally constrained manner, using a lookup table-based inverse model. The obtained optical properties were analyzed and compared among different tumor groups. The calculated parameters of the absorption and reduced scattering coefficients were subsequently used for detection of malignant skin and subcutaneous tumors. The detection sensitivity and specificity of malignant tumors *ex vivo* were 90.0% and 73.5%, respectively, while corresponding detection sensitivity and specificity of malignant tumors *in vivo* were 88.4% and 54.6%, respectively. The obtained results show that the DRS is a promising noninvasive optical technique for detection and classification of malignant and benign canine skin and subcutaneous tumors. The method should be further investigated on tumors with common origin. [DOI: 10.1117/1.JBO.20.3.037003]

Keywords: diffuse reflectance spectroscopy; veterinary oncology; diagnosis; skin and subcutaneous tumors.
Paper 140786R received Nov. 28, 2014; accepted for publication Feb. 12, 2015; published online Mar. 9, 2015.

1 Introduction

Cancer is the main cause of companion animal morbidity and mortality.[1,2] Canine mortality rate due to neoplasms is estimated to be around 18%. The mortality rate further increases with age and is estimated to be around 45% for animals older than 10 years.[3] Studies have shown that 30% of all canine neoplasms appear on the skin.[4,5] Among the most common skin and subcutaneous tumors are mast cell tumor (MCT, 16.8%), lipoma (8.5%), histiocytoma (8.4%), and perianal gland adenoma (7.8%).[6] The existing evaluation of skin tumors is based on a complete review of the patient's history, physical examination, fine-needle aspiration or direct impression, and cytological examination of the sample, staging, and sometimes histopathology.[6] Such evaluation can often be unpleasant for the animal and its owner and requires an experienced veterinarian in order to reach a proper diagnosis. Therefore, a lot of effort is being devoted to the development of novel noninvasive tools aiding the diagnostic process or providing the means for rapid screening of patients that can lead to early tumor detection, before the invasive or metastatic disease develops.

There are a number of noninvasive optical techniques aiding the tumor diagnosis and therapy that are being developed and used in human medicine.[7–9] The main objective of these techniques is to provide relevant quantitative data useful for physicians and others working in oncology. Among the optical techniques, diffuse reflectance spectroscopy (DRS) is convenient for collecting spectral information from the skin surface.[10] DRS spectra are acquired by illuminating the tissue surface with a broadband visible (VIS) or near-infrared (NIR) source and collecting the partially reflected, absorbed, and scattered light forming the unique diffuse reflectance spectrum. With proper analysis of the acquired DRS spectra, the absorption and scattering properties (coefficients) of the tissue can be derived. The tissue absorption depends on the concentration of chromophores (water, hemoglobin, lipids, and melanin) that selectively absorb light of specific spectral bands, while the scattering depends on the tissue morphology. As the tumors chemically and morphologically differ from normal tissue, DRS potentially provides the means to determine the extent and the tumor type. Due to the increased angiogenesis and edema, tumor tissue exhibits higher water and hemoglobin contents, while the increased metabolic rate results in a lower lipid concentration and oxygen saturation. Tumors consist of mutated cells and exhibit increased cellularity and consequently different tissue morphology.[11]

Several studies reported on the use of DRS for diagnosis and therapy of human skin, breast, cervix uteri, brain, head and neck, bronchial mucosa, prostate, pancreas, colon, and rectum cancers. DRS as a phototherapeutic application was used for optimizing the biological effect, accurate dosimetry, and monitoring of treatment progress and efficacy.[11] The reported DRS methods for detection of skin tumors exhibited sensitivity and specificity

*Address all correspondence to: Blaž Cugmas, E-mail: blaz.cugmas@fe.uni-lj.si

1083-3668/2015/$25.00 © 2015 SPIE

between 64% and 92%, and 72% and 92%, respectively.[8] The first extensive study focused on classification of different skin lesions, namely dysplastic and common nevi, actinic and seborrheic keratoses, lentigines, and basal cell carcinoma.[12] Several studies attempted to differentiate melanoma from other skin lesions (dysplastic and common nevus, actinic and seborrheic keratoses, and basal and squamous cell carcinoma)[13–18] or to detect nonmelanoma lesions.[19,20] Canpolat et al.[17] proposed a method for detecting positive surgical margins. Furthermore, DRS was also used for the detection of head, neck, and breast tumors.[21–24]

Existing canine tumor evaluation requires an experienced veterinarian and often involves invasive fine-needle aspiration, which can be an unpleasant procedure for the patient and its owner. In this study, we evaluate DRS as a noninvasive diagnostic aid for *ex vivo* and *in vivo* detection of canine skin and subcutaneous tumors by using a set of optical properties derived from the acquired DRS spectra. To the best of our knowledge, DRS has not yet been used in veterinary oncology.

2 Material and Methods

2.1 *Clinical Study Design*

The patients underwent prearranged normal surgical procedures for skin and subcutaneous tumor excision. First, the patient was put under general anesthesia followed by a preoperative skin preparation. After precise hair clipping, two sets of *in vivo* DRS NIR spectra were acquired (Tumors *In Vivo*). The first set was acquired from the skin above the tumor and the second set was acquired circularly from the normal skin around the tumor. The preoperative skin preparation was followed by cleaning and disinfecting the surgical field and finally performing the excision. The excised tumors were halved and put into physiological solution (as in Ref. 25). One half was immediately taken to the laboratory where *ex vivo* VIS and NIR DRS spectra were acquired across the entire surface of the surgical section (Tumors *Ex Vivo*). Additionally, spectra of unchanged (normal) canine skin were acquired (Skin *Ex Vivo*). Prior to measurements, the subcutaneous fat was removed from the skin samples. Finally, the remaining excised tumor samples were put in formalin solution and sent for histopathological examination.

From the 31 tumor samples studied *in vivo*, 10 were benign and 21 were malignant. The most common tumors were carcinomas (8), sarcomas (6), epiteliomas (4), and MCTs (4). The *ex vivo* study included 47 tumor samples in which 18 were benign and 29 were malignant. The most common tumors were carcinomas (14), sarcomas (8), epiteliomas (7), lipomas (6), and MCTs (5). Fifteen skin samples were investigated *ex vivo* by VIS and NIR DRS. Hemoglobin and melanin concentrations and oxygen saturation of tumor and skin samples were estimated from the VIS spectra, while the concentration of water and lipids was estimated from the NIR spectra (Table 1). The average thickness of skin samples was 2.3 mm, with a standard deviation of 0.5 mm. The skin samples were divided into three pigmentation groups: (1) lightly pigmented skin, (2) darkly pigmented skin, and (3) other skin samples which had different shades of gray or brown color. The three pigmentation groups were introduced for easier comparison with other studies, mostly performed on human skin.

Table 1 List of chromophores used in the visible (VIS) and near-infrared (NIR) spectral ranges [Eq. (1)].

Sample	Spectral range	Chromophores
Skin *ex vivo*	VIS	Melanin and hemoglobin
	NIR	Water and melanin
Tumors *ex vivo*	VIS	Hemoglobin
	NIR	Water and lipids
Tumors *in vivo*	NIR	Water, melanin, and lipids

2.2 *Instrumentation and Data Processing*

Spectra were acquired by a commercial VIS spectrometer (AvaSpec-2048-TEC-FT, 177 to 1098 nm, Avantes, Apeldoorn, The Netherlands) and a commercial NIR spectrometer (NIR-512L-1.7T1, 901 to 1685 nm, Control Development, South Bend, Indiana). A broadband halogen light source (AvaLight-Hal LS, Avantes) and a stainless steel fiber optic diffuse reflectance probe (FCR-7IR400-2-ME, Avantes), consisting of one detection and six illumination fibers (400 μm core diameter, NA = 0.22, 478-μm source-detector separation), were employed. The diameter of the probe was 6.35 mm corresponding to 31.7 mm^2 of contact area. All the acquired spectra were calibrated using a standard diffuse reflectance tile (Spectralon, Labsphere, North Sutton, New Hampshire). Due to the poor sensitivity of the employed VIS and NIR sensor arrays at the lower and the upper ends of the spectral range, only the spectral ranges from 400 to 900 nm and from 920 to 1600 nm were used, respectively.

Tissue optical properties in terms of absorption and reduced scattering coefficients (ARSCs) were determined by a lookup table (LUT)-based inverse model.[26] Briefly, measuring the optical properties *in vivo* by a DRS probe can be performed only indirectly, through a model which estimates the optical properties from the acquired DRS spectra. The model can be represented by a complex mathematical formulation or a surface spanned over the domain of optical properties (LUT). LUT is built experimentally by acquiring diffuse reflectance spectra of optical phantoms with exactly defined optical properties. In this way, diffuse reflectance spectra can be estimated for each combination of sample absorbance and reduced scattering coefficients. Solving the inverse problem for a DRS tissue spectrum finds the optical properties by maximizing similarity between the synthetic LUT-based and the acquired spectrum. The optical phantoms that were used to derive the LUT consisted of water, violet ink molecular absorber (Brause&Cie, G.Lado, Paris, France), Intralipid 20% solution (Sigma-Aldrich, St. Louis, Missouri), and polystyrene spheres (Polybead Microspheres 1.00 μm, prod. 07310, Polysciences, Warrington, Florida) scatterers. The ink selection was largely based on the study of Nichols et al.,[27] with the goal of reducing the number of required phantoms while preserving the full range of optical properties. The absorption spectrum of ink was assessed by measuring the attenuation of a collimated beam over a 5-mm

quartz cuvette filled with the ink solution. On the other side, the reduced scattering coefficient of the Intralipid 20% solution was found in the literature,[28] while the reduced scattering coefficient of the microsphere solution was calculated according to the Mie theory.[29]

The calculated LUT model was valid for the absorption coefficient [Eq. (1)] in the range from 0.01 to 125.11 cm^{-1} and in the range from 0.01 to 35.11 cm^{-1} for the VIS and NIR spectral ranges, respectively. Analogically, the valid range of the reduced scattering coefficient [Eq. (2)] was from 0.8 to 142.5 cm^{-1} for the VIS and from 0.5 to 72.5 cm^{-1} for the NIR spectral range. For validation purposes,[26,27] four extra phantoms based on 0.51-μm polystyrene microspheres (Polybead Microspheres 0.51 μm, prod. 07307, Polysciences) and red ink (Brause&Cie, G. Lado) were created. The mean relative errors of the estimated absorption and scattering coefficients in the VIS spectral range were 12.8% and 7.2%, respectively. The corresponding mean relative errors of the estimated absorption and scattering coefficients in the NIR spectral range were 5.7% and 12.8%, respectively.

The ARSCs of the tissue were calculated in a spectrally constrained manner. The absorption coefficient μ_a (cm^{-1}) was modeled as a linear combination of the chromophore concentrations:[30,31]

$$\mu_a(\lambda) = f_w\mu_{a,w} + C_{\mathrm{mel}}\varepsilon_{\mathrm{mel}} + f_{\mathrm{lip}}\mu_{a,\mathrm{lip}} + f_{\mathrm{hem}}(\alpha\mu_{a,\mathrm{oxyhem}} + (1-\alpha)\mu_{a,\mathrm{deoxyhem}}), \quad (1)$$

where $\mu_{a,w}$,[32] $\mu_{a,\mathrm{lip}}$,[33,34] $\mu_{a,\mathrm{oxyhem}}$, and $\mu_{a,\mathrm{deoxyhem}}$[35] are the wavelength-dependent absorption coefficients (cm^{-1}) of water, lipids, oxyhemoglobin, and deoxyhemoglobin, respectively, and $\varepsilon_{\mathrm{mel}}$[36,37] is the extinction coefficient of melanin [$cm^{-1}/(\mathrm{mmol/l})$]. On the other hand, f_w, f_{lip}, and f_{hem} are the dimensionless volume fractions (relative concentrations) of pure water, lipids, and hemoglobin, respectively, C_{mel} is the melanin concentration (mmol/l), and α is the oxygenation fraction (i.e., saturation). In order to simplify the comparison with other studies, hemoglobin mass concentration $C_{m.\mathrm{hem}}$ was calculated as $C_{m.\mathrm{hem}} = 150\ \mathrm{g/l}\, f_{\mathrm{hem}}$, assuming a whole blood hemoglobin mass concentration of 150 g/l. Due to the instrumentation and sample properties, only a subset of chromophores was used for a particular combination of sample and spectral range (Table 1).

The reduced scattering coefficient was modeled according to the wavelength-dependent power law:[26,38]

$$\mu_s'(\lambda) = u\left(\frac{\lambda}{\lambda_0}\right)^{-v}, \quad (2)$$

where u is the scattering magnitude and v is the scattering power. The value of parameter λ_0 was set to 630 nm[26] and 1000 nm for the VIS and NIR spectral ranges, respectively. The effective penetration depth (δ), where the intensity of light entering a semi-infinite medium is attenuated by a factor of e, was calculated according to[38,39]

$$\delta(\lambda) = \frac{1}{\mu_{\mathrm{eff}}} = \frac{1}{\sqrt{3\mu_a[\mu_a + \mu_s']}}, \quad (3)$$

where μ_{eff} is the effective attenuation coefficient.

In this study, the classification between different tissues was performed by a quadratic discriminant analysis (QDA)[40] employing sequential forward-floating selection (SFFS) feature selection algorithm.[41] QDA has been frequently employed in similar human studies; therefore, the same classification scheme was adopted for straightforward comparison of the obtained results. The estimated parameters of the ARSCs (f_w, C_{mel}, f_{lip}, $C_{m.\mathrm{hem}}$, α, u, and v) served as the feature vectors. The absolute values of parameters were used for the *ex vivo* samples, while the normalized parameters ($\mathrm{ARSC_{rel}}$) calculated as the relative differences between the normal and tumor skin parameters were used for *in vivo* samples:

$$\mathrm{ARSC_{rel}} = \frac{\mathrm{ARSC_{tum}} - \mathrm{ARSC_{nor}}}{\mathrm{ARSC_{nor}}}, \quad \text{where ARSC} \in \{f_w, C_{\mathrm{mel}}, f_{\mathrm{lip}}, u, v\}, \quad (4)$$

where $\mathrm{ARSC_{nor}}$ and $\mathrm{ARSC_{tum}}$ are the values of parameters estimated for the skin above normal tissue and tumor, respectively. With respect to the number of available samples, a leave-one-out cross-validation was selected to evaluate the classification between the benign and malignant tumors. The sensitivity for each of the two tissue classes was calculated as the corresponding true positive rate. Specificity, on the other hand, was defined as the true negative rate.

3 Results

In order to gain basic information on the optical properties of the tissues used in this study, the DRS spectra of canine skin samples were analyzed first (Skin *Ex Vivo*, see Sec. 2.1) (Fig. 1). Next, the optical properties of the *ex vivo* and *in vivo* tumor samples were assessed (Tumors *Ex Vivo* and *In Vivo*). Finally,

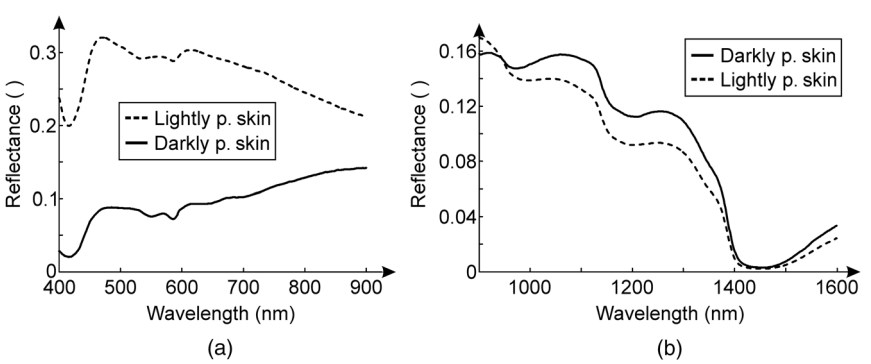

Fig. 1 Mean *ex vivo* diffuse reflectance spectra of the lightly and darkly pigmented skin in the (a) visible (VIS) and (b) near-infrared (NIR) spectral ranges.

Table 2 Skin *ex vivo*. Mean values of the ARSC parameters obtained for the normal canine skin samples.

ARSC parameter	Spectral range	Value
f_w	NIR	81.40%
C_{mel} (lightly pigmented skin)	VIS	0.26 mmol/l
C_{mel} (darkly pigmented skin)	VIS	2.22 mmol/l
$C_{m.hem}$	VIS	1.07 g/l
α	VIS	46%
u	VIS	11.54 cm^{-1}
	NIR	11.02 cm^{-1}
v	VIS	1.03
	NIR	0.20

Table 3 Tumors *ex vivo*. Mean values of the ARSC parameters estimated from the *ex vivo* DRS spectra of benign and malignant tumors.

ARSC parameter	Spectral range	Benign	Malignant
f_w	NIR	61.2% (81.6%)[a]	82.4%
$C_{m.hem}$	VIS	0.62 g/l (1.97 g/l)[a]	7.93 g/l
f_{lip}	NIR	26.94% (11.13%)[a]	8.78%
α	VIS	48% (56%)[a]	53%
u	VIS	7.69 cm^{-1} (10.26 cm^{-1})[a]	11.16 cm^{-1}
	NIR	10.53 cm^{-1} (11.81 cm^{-1})[a]	9.25 cm^{-1}
v	VIS	0.62 (1.08)[a]	1.07
	NIR	0.63 (0.99)[a]	0.92

[a]Excluding lipomas.

detection of malignant tumors was evaluated by employing a QDA-based classifier.

Table 2 lists the mean values of canine skin ARSC parameters. The average water volume fraction in the skin samples was 81.4%. Darkly pigmented skin contained almost 10 times more melanin than lightly pigmented skin. The average hemoglobin mass concentration was 1.07 g/l and saturation was 46%. Scattering magnitude u was similar for the VIS and NIR spectral ranges, however, scattering was less dependent on the wavelength in the NIR spectral range, where the average scattering power v was lower. Finally, the effective penetration depth was estimated from the calculated ARSCs of the darkly and lightly pigmented skin [Eq. (3)]. The effective penetration depth and the average skin thickness are shown in Fig. 2.

The ARSC parameters calculated for tumors *ex vivo* are summarized in Table 3 and plotted in Fig. 3. With exception to lipomas, the estimated parameters of the benign and malignant tumor samples exhibited similar values. The water volume fraction (f_w) was around 82%, saturation was slightly above 50%, and lipid relative concentration (f_{lip}) was between 8.78% and 11.13%. The value of parameter u ranged from 9.25 to 11.81 cm^{-1}, and the value of parameter v was close to 1.0. However, benign tumors contained 0.62 g/l of hemoglobin and malignant tumors contained 7.93 g/l of hemoglobin. The difference was statistically significant (unpaired t-test: $p = 0.01$).

The mean ARSC parameters of individual tumor groups *ex vivo* are listed in Table 4. The water volume fraction of most tumor groups was around 80%. Lipomas, on the other hand, contained 30.9% of water and 55.6% of lipids. Lipomas also exhibited less scattering (lower u) and lower dependence of the scattering on the wavelength (lower v) than the other tumor groups. Hemangiopericytoma that represented the majority of sarcomas exhibited the highest average mass concentration of hemoglobin, i.e., 16.0 g/l. Differences in the values of other parameters were not significant.

The *in vivo* DRS NIR spectra above the normal and tumor tissues were acquired immediately before the tumor excision, when the patients were already under general anesthesia. The reflectance observed above the tumors was, in general, lower than the reflectance observed above the normal subcutaneous tissue (Fig. 4). The calculated normalized [Eq. (4)] values of parameters for benign and malignant tumor groups are listed in Table 5. The results show that the parameter values above

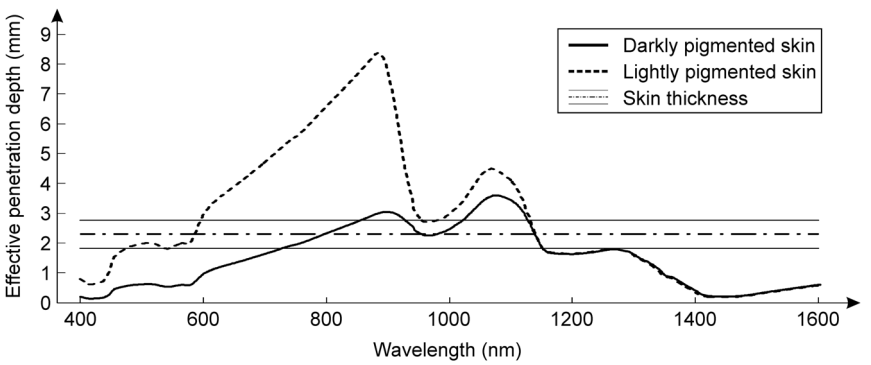

Fig. 2 Skin *ex vivo*. Effective penetration depth of the lightly (dashed line) and darkly (full line) pigmented canine skin. Mean skin thickness and corresponding standard deviation are represented by a dash-dotted and two full lines, respectively.

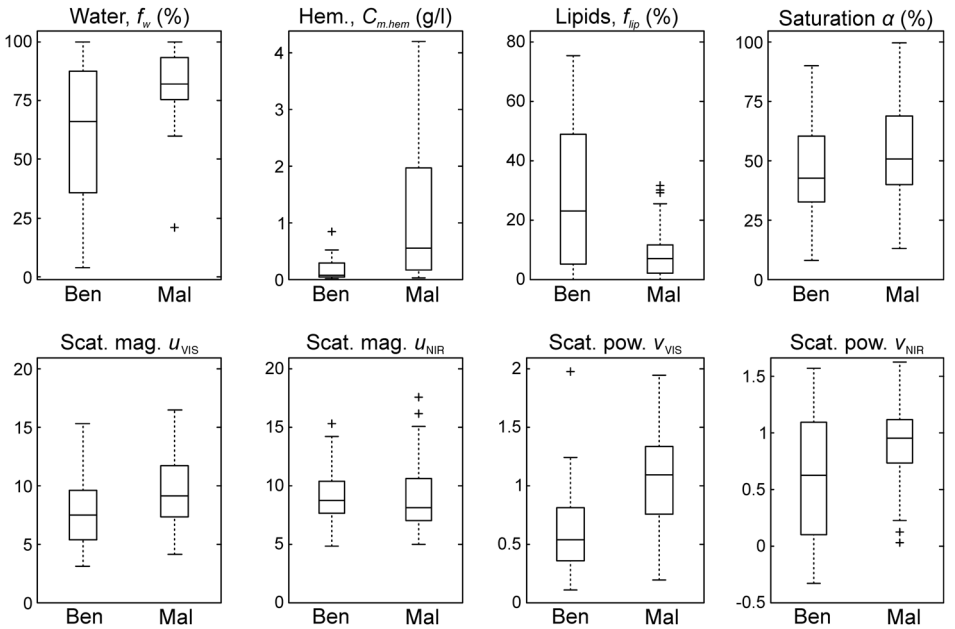

Fig. 3 Box-and-whisker plots of the ARSC parameters for the benign (Ben) and malignant (Mal) tumors.

Table 4 Tumors *ex vivo*. Mean values of the ARSC parameters estimated from the *ex vivo* diffuse reflectance spectra of tumors.

ARSC parameter	Spectral range	Epiteliomas	Carcinomas	Sarcomas	Mast cell tumor (MCT)	Lipomas
f_w	NIR	79.3%	84.3%	82.8%	79.0%	30.9%
$C_{m.\mathrm{hem}}$	VIS	0.52 g/l	1.25 g/l	16.01 g/l	0.41 g/l	0.15 g/l
f_{lip}	NIR	9.96%	10.54%	8.20%	7.03%	55.63%
α	VIS	55%	64%	41%	49%	45%
u	VIS	9.82 cm^{-1}	12.50 cm^{-1}	10.72 cm^{-1}	11.70 cm^{-1}	6.80 cm^{-1}
u	NIR	13.20 cm^{-1}	8.05 cm^{-1}	9.76 cm^{-1}	8.46 cm^{-1}	8.63 cm^{-1}
v	VIS	0.96	1.07	1.03	1.41	0.46
v	NIR	1.02	0.94	0.96	0.82	0.08

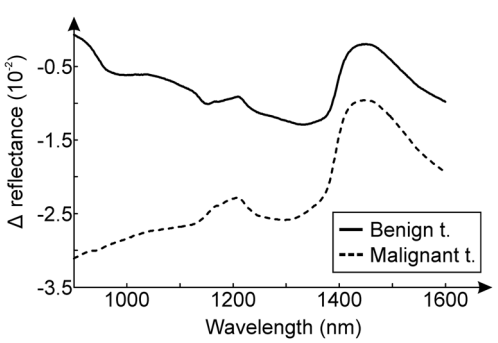

Fig. 4 Mean differences between the diffuse reflectance spectra of benign and malignant tumors ($R_{\mathrm{tum}} - R_{\mathrm{nor}}$) *in vivo*.

Table 5 Tumors *in vivo*. Mean relative changes of the ARSC parameters, with respect to the surrounding normal skin, estimated from the *in vivo* NIR diffuse reflectance spectra of benign and malignant tumors.

$\mathrm{ARSC}_{\mathrm{rel}}$ parameter	Spectral range	Benign (%)	Malignant (%)
f_w	NIR	+74.0	+25.6
C_{mel}	NIR	+48.7	+54.3
f_{lip}	NIR	+34.7	+6.3
u	NIR	+1.7	−11.3
v	NIR	+57.1	+23.2

Table 6 Sensitivity and specificity of classification between the malignant and benign tumors based on (I) *ex vivo* NIR and VIS ARSC parameters (Table 3), (II) *ex vivo* NIR ARSC parameters f_w, f_{lip}, u_{NIR}, and v_{NIR}, (III) *in vivo* $ARSC_{rel}$ parameters [Eq. (4)], and (IV) reduced set of *in vivo* NIR spectra acquired above the tumor tissue [$ARSC_{tum}$ from Eq. (4)].

Classification	Features	Spectral range	Sensitivity (%)	Specificity (%)
I	*Ex vivo* ARSC	VIS and NIR	90.0	73.5
II	*Ex vivo* ARSC *(NIR)*	NIR	91.7	56.7
III	*In vivo* $ARSC_{rel}$	NIR	88.4	54.6
IV	*In vivo* $ARSC_{tum}$	NIR	55.5	21.2

the tumor were generally higher than the parameter values observed above the surrounding healthy tissue.

The four employed classification schemes were used to discriminate malignant tumors from benign tumors (Table 6). Classification I of malignant tumors, based on the ARCS parameters extracted from the *ex vivo* DRS spectra (Table 3), exhibited sensitivity and specificity of 90.0% and 73.5%, respectively. The water volume fraction f_w and scattering magnitude u_{NIR} were selected by the SFFS algorithm as the most prominent classification features. Classification III of malignant tumors, based on the $ARSC_{rel}$ parameters estimated from the *in vivo* DRS spectra [Eq. (4)], exhibited sensitivity and specificity of 88.4% and 54.6%, respectively. These results were similar to the sensitivity (91.7%) and specificity (56.7%) of Classification II obtained by the ARSC parameters f_w, f_{lip}, u_{NIR}, and v_{NIR} (Table 3) estimated from the *ex vivo* NIR DRS spectra. Finally, Classification IV was performed by excluding the spectra of healthy surrounding tissue from the training set, i.e., using only the $ARSC_{tum}$ parameters from Eq. (4). The tumor classification sensitivity and specificity dropped to merely 55.5% and 21.2%, respectively.

4 Discussion

4.1 *Skin Ex Vivo*

Since measurements were conducted shortly after excision, the gross postmortem and histological changes should have limited effect on the results.[42] Average water volume fraction in the skin was 81.4%, which is slightly higher than the values reported in the literature, where the water volume fraction was estimated to be in the range from 58.6% to 72.1%.[43,44] The higher water concentration could be explained by two reasons. First, the skin samples were kept in a saline solution that could lead to the absorption of some extra water into the sample. Second, in order to assure adequate light coupling between the sample and the DRS probe, the sample surface was not wiped and a thin layer of water remained between the probe and the sample. The results show that lightly pigmented skin exhibited higher mean water content (88.5%) than the darkly pigmented skin (77.8%). The results could be explained by the lower absorption of NIR light in the lightly pigmented samples with low melanin concentration, which result in more light reaching the dermis that has higher water content than the epidermis.[45]

Average melanin concentration of lightly pigmented canine skin (Table 2, Fig. 1) was 0.26 mmol/l. Under the assumption that the molecular weight of eumelanin monomer (DHI) is 178 g/mol,[37] the average melanin mass concentration of lightly pigmented skin was estimated to 46.3 mg/l. Analogically, the concentration of darkly pigmented skin was estimated to be about 10-fold higher, i.e., 2.22 mmol/l or 395.2 mg/l. Validation of these results is not an evident task, since eumelanin is an extremely heterogeneous macromolecule consisting of dihydroxyindole (DHI)- and dihydroxyindole -2-carboxylic acid-derived units.[46] One of the methods is to quantify the melanin content by weight. It has been reported that white and dark human skin contain 0.008% and 0.023% melanin, respectively.[47] Assuming the density of human skin is around 1050 g/l,[48] the melanin concentration in lightly and darkly pigmented human skin can be estimated to 84.0 and 241.5 mg/l, respectively. Furthermore, the melanin concentrations were also estimated for the human epidermis.[30] However, these results excluded the melanin-free dermis. Therefore, the reported results need to be adjusted by the ratio between the average thickness of the epidermis (0.06 mm) and the whole skin (2.3 mm), obtaining the corrected melanin concentrations of 115.0 and 443.5 mg/l for the lightly and darkly pigmented human skin, respectively. In contrast, some studies that used DRS[49] to estimate the melanin concentration reported substantially higher values of 1.9 and 13.0 mg/ml for the lightly and darkly pigmented human skin, respectively.

The calculated average hemoglobin mass concentration in the *ex vivo* canine skin samples was 1.07 g/l and the saturation was 46%. The majority of the existing DRS-based estimates of the skin hemoglobin content and saturation were performed *in vivo*.[30,50,51] The reported hemoglobin concentrations were in the range from 0.65 to 3.33 g/l and the saturation was in the range from 60% to 99%. The slightly lower saturation level obtained in this study can be attributed to the *ex vivo* measurements.

Even though a fixed value of the scattering power v modeling the reduced scattering coefficient [Eq. (3)] was used in one study,[30] it was shown that the scattering coefficient of the whole skin, including the dermis, is wavelength dependent.[25] The wavelength-dependent nature of the scattering coefficient was also confirmed by the results of this study. The average scattering power in the VIS spectral range was 1.03 and gradually dropped to 0.20 in the NIR spectral range. As discussed in Ref. 25, wavelength-independent Mie scattering, resulting from the collagen and elastin bundles of size in the order of the light wavelength, is dominant in the NIR spectral range. However, the length of a single collagen and elastin fiber is between 60 and 100 nm, which is lower than the wavelengths of VIS light. Therefore, the wavelength-dependent Rayleigh scattering dominates the VIS spectral range.

The cumulative attenuation of light by chromophores in the tissue can be quantified by the effective penetration depth [Fig. 2, Eq. (3)]. The estimated effective penetration depth of canine skin was similar to the results reported for the human skin.[25] The effective penetration depth of the lightly pigmented canine skin peaked at 885 nm with the value of 8.4 mm. At this wavelength, the cumulative absorption of all the three major chromophores (water, hemoglobins, and melanin) is the lowest. The effective penetration depth of lightly pigmented skin exceeded the average skin thickness in the spectral range from

587 to 1140 nm. The light of shorter wavelengths was strongly absorbed by the hemoglobins and melanin, while the light of longer wavelengths was absorbed by water. The melanin content of darkly pigmented canine skin substantially increased the absorption coefficient. Consequently, the effective penetration depth exceeded the average skin thickness in the reduced spectral range from 800 to 1140 nm.

4.2 *Tumors Ex Vivo*

The ARSC parameters estimated from the *ex vivo* VIS and NIR spectra are summarized in Table 3 and shown in Fig. 3. On average, the hemoglobin concentration observed in malignant tumors was significantly (unpaired t-test: $p = 0.01$) higher than in benign tumors. The difference in hemoglobin content was expected as the active angiogenesis in malignant tumors results in higher microvessel density.[52–54]

The mean values of ARSC parameters obtained for the individual tumor groups are listed in Table 4. As expected, the values obtained for lipomas stand out. Lipomas consist of mature unilocular adipocytes that measure up to 120 μm in diameter and are occupied by a single, large lipid droplet.[55] The lipoma cells are histologically identical to those found in normal adipose tissue, where the lipid volume fraction is around 80%.[56] The results obtained in this study show that the lipomas contain 55.6% lipids. The slightly lower values could be attributed to the same reason as already pointed out in Sec. 4.1 on the skin canine analysis. Samples were kept in a saline solution and were not wiped prior to the acquisition of DRS spectra. Consequently, the estimated water concentration was higher and the concentration of other chromophores was lower. In comparison with other tumor groups, lipomas exhibited lower scattering (lower u) that was less dependent on the wavelength (lower v). The observations could be explained by the displacement of adipocyte cell nucleus to the periphery by the lipid droplet. Additionally, the surrounding cytoplasm contains small Golgi complex, mitochondria, rough endoplasmic reticulum, and microfilaments. On the other hand, hemangiopericytoma are tumors composed of blood vessel mural cells,[55] hence sarcomas exhibited the highest average amount of hemoglobin, i.e., 16.01 g/l. The spectral influence of hemoglobin, lipids, and water of some prominent tumor groups can be seen in Fig. 5.

4.3 *Tumors In Vivo*

The mean relative changes of ARSC parameters estimated from the *in vivo* DRS spectra are mostly positive (Table 5). The water volume fraction increased for all the tumor groups, however, the increase was most prominent for benign tumors (74.0%). Even though the water content increase observed for benign tumors was expected, it was not expected to significantly deviate from the increase observed for malignant tumors. Considering the *ex vivo* results (Table 3), we believe that the characteristics of tumor mass are not the only factor responsible for the observed increase [Eq. (4), Table 5]. At least two additional factors could significantly contribute to the effect. First, the skin above a subcutaneous tumor could be modified as well. For example, the tumor samples, used in this study, did not contain melanin. Therefore, the increase in C_{mel} (Table 5) must be attributed solely to the changes in the skin above the tumor. Second, the changes also depend on the surrounding subcutaneous tissue. For example, many tumors in bitches appear on the mammary gland. According to the human study,[43] the water volume fraction in mammary tissue varies substantially, i.e., in the range from 30.2% to 72.6%. Therefore, the exact location of the tumor can significantly affect the measurements. An attempt was made to minimize the impact of the surrounding tissue on the measurements by acquiring spectra from several circularly spread locations around the tumor. However, it seems that this approach alone was insufficient.

An increase in the volume fraction of lipids was observed for both the benign and malignant tumors. The scattering parameter u decreased for malignant tumors indicating lower scattering. The observed increase in the value of parameter v indicates the stronger wavelength dependence of the scattering in the benign and malignant tumors. This could be attributed to the increase in the content of small particles (e.g., organelles and fibers which cause higher Rayleigh scattering) and decrease in the content of large particles (e.g., lipid droplets which cause lower Mie scattering).

4.4 *Classification*

Ex vivo detection of malignant tumors (Classification I in Table 6) exhibited sensitivity and specificity of 90.0% and 73.5%, respectively. The obtained results are similar to the results reported by the majority of human studies.[8] Detection of tumors based on *in vivo* DRS spectra (Classification III) performed worse. The obtained sensitivity and specificity were 88.4% and 54.6%, respectively. However, the classification was based solely on the NIR spectral range. If these results are compared with the classification results obtained by the NIR *ex vivo* spectra (Classification II, sensitivity = 91.7% and specificity = 56.7%), it can be seen that the *in vivo* results follow the trend of the *ex vivo* results. Therefore, we believe that

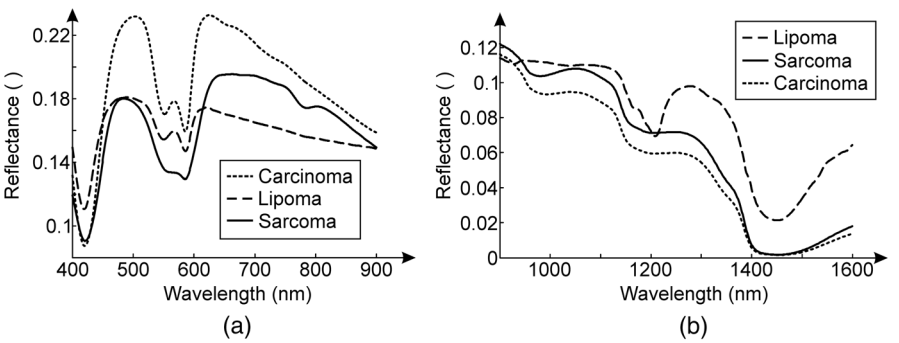

Fig. 5 Mean *ex vivo* diffuse reflectance spectra of the selected tumor groups in the (a) VIS and (b) NIR spectral ranges.

combining the NIR and VIS spectral ranges would lead to similar *in vivo* tumor detection results as observed for the *ex vivo* samples. However, due to hygienic, medical, and technical reasons, only one spectrometer could be used in the preoperative area. As the VIS spectral range is strongly affected by the melanin absorption, the NIR spectral range was selected. Nevertheless, using the relative changes of ARSC parameters [Eq. (4)] proved useful for malignant tumor detection. On the other hand, excluding the spectra of surrounding healthy tissue from the classification, the tumor detection sensitivity and specificity dropped to merely 55.5% and 21.2%, respectively (Classification IV).

5 Conclusions

In this study, we showed that canine skin has similar optical properties to human skin. The main chromophores, namely water, melanin, and hemoglobin, can heavily reduce the effective penetration depth. Malignant tumors were successfully detected *ex vivo* and *in vivo*, based on the chromophore concentrations and scattering parameters that significantly differed from benign tumors. Lipomas strongly differed from the other tumor groups by their distinct structure. We assume that *in vivo* detection of malignant tumors was not only based solely on the tumor characteristics, but also based on the surrounding tissue and changes in the skin above the tumors.

The future work should focus on the detection/differentiation of tumors with common histological origin, i.e., lipomas—liposarcomas, with the aim of providing more precise explanations of the specific changes in the diffuse reflectance spectra. Better understanding of these changes could further improve the sensitivity and specificity of malignant tumor detection and lead to the application of DRS in clinical veterinary oncology. In comparison with the existing tumor evaluation procedures (cytology or even histopathology), DRS would be fully noninvasive, less time consuming, and much more cost-effective for the clinics and owners, providing quantitative evaluation results that are not prone to human error.

Acknowledgments

This work was supported by the Slovenian Research Agency under the Grants L2-4072, L2-2023, and P2-0232. We gratefully thank the team of the Clinic for Small Animal Medicine and Surgery from the Veterinary Faculty for all the help and technical support.

References

1. B. Bonnett et al., "Mortality in over 350,000 insured Swedish dogs from 1995–2000: I. Breed-, gender-, age- and cause-specific rates," *Acta Vet. Scand.* **46**(3), 105–120 (2005).
2. S. Withrow, D. Vail, and R. Page, "Why worry about cancer in companion animals?" in *Withrow & MacEwen's Small Animal Clinical Oncology*, S. Withrow, D. Vail, and R. Page, Eds., 5th ed., pp. xv–xvi, W.B. Saunders, St. Louis, Missouri (2013).
3. R. Bronson, "Variation in age at death of dogs of different sexes and breeds," *Am. J. Vet. Res.* **43**(11), 2057–2059 (1982).
4. H. Kaldrymidou et al., "Prevalence, distribution and factors associated with the presence and the potential for malignancy of cutaneous neoplasms in 174 dogs admitted to a clinic in Northern Greece," *J. Vet. Med. A* **49**(2), 87–91 (2002).
5. B. Pakhrin et al., "Retrospective study of canine cutaneous tumors in Korea," *J. Vet. Sci.* **8**(3), 229–236 (2007).
6. L. Hauck, "Tumors of the skin and subcutaneous tissues," in *Withrow & MacEwen's Small Animal Clinical Oncology*, S. Withrow, D. Vail, and R. Page, Eds., 5th ed., pp. 375–401, W.B. Saunders, St. Louis, Missouri (2013).
7. D. J. Evers et al., "Optical spectroscopy: current advances and future applications in cancer diagnostics and therapy," *Future Oncol.* **8**(3), 307–320 (2012).
8. M. Calin et al., "Optical techniques for the noninvasive diagnosis of skin cancer," *J. Cancer Res. Clin. Oncol.* **139**(7), 1083–1104 (2013).
9. J. Q. Brown et al., "Quantitative optical spectroscopy: a robust tool for direct measurement of breast cancer vascular oxygenation and total hemoglobin content in vivo," *Cancer Res.* **69**(7), 2919–2926 (2009).
10. T. M. Bydlon et al., "Chromophore based analyses of steady-state diffuse reflectance spectroscopy: current status and perspectives for clinical adoption," *J. Biophotonics* **8**(1–2), 9–14 (2015).
11. V. R. Kondepati, H. M. Heise, and J. Backhaus, "Recent applications of near-infrared spectroscopy in cancer diagnosis and therapy," *Anal. Bioanal. Chem.* **390**(1), 125–139 (2008).
12. L. M. McIntosh et al., "Towards non-invasive screening of skin lesions by near infrared spectroscopy," *J. Invest. Dermatol.* **116**(1), 175–181 (2001).
13. B. W. Murphy et al., "Toward the discrimination of early melanoma from common and dysplastic nevus using fiber optic diffuse reflectance spectroscopy," *J. Biomed. Opt.* **10**(6), 064020 (2005).
14. N. Rajaram et al., "Design and validation of a clinical instrument for spectral diagnosis of cutaneous malignancy," *Appl. Opt.* **49**(2), 142–152 (2010).
15. G. Zonios et al., "In vivo optical properties of melanocytic skin lesions: common nevi, dysplastic nevi and malignant melanoma," *Photochem. Photobiol.* **86**(1), 236–240 (2010).
16. A. Garcia-Uribe et al., "In vivo diagnosis of melanoma and nonmelanoma skin cancer using oblique incidence diffuse reflectance spectrometry," *Cancer Res.* **72**(11), 2738–2745 (2012).
17. M. Canpolat et al., "Diagnosis and demarcation of skin malignancy using elastic light single-scattering spectroscopy: a pilot study," *Dermatol. Surg.* **38**(2), 215–223 (2012).
18. L. Lim et al., "Clinical study of noninvasive in vivo melanoma and nonmelanoma skin cancers using multimodal spectral diagnosis," *J. Biomed. Opt.* **19**(11), 117003 (2014).
19. Y. Jiao et al., "Interrogation of skin pathology using elastic scattering spectroscopy," *Head Neck Oncol.* **1**(Suppl 1), O19 (2009).
20. T. Upile et al., "Elastic scattering spectroscopy in assessing skin lesions: an 'in vivo' study," *Photodiagn. Photodyn.* **9**(2), 132–141 (2012).
21. B. J. Tromberg et al., "Imaging in breast cancer—diffuse optics in breast cancer: detecting tumors in pre-menopausal women and monitoring neoadjuvant chemotherapy," *Breast Cancer Res.* **7**(6), 279–285 (2005).
22. U. Sunar et al., "Noninvasive diffuse optical measurement of blood flow and blood oxygenation for monitoring radiation therapy in patients with head and neck tumors: a pilot study," *J. Biomed. Opt.* **11**(6), 064021 (2006).
23. M. D. Keller et al., "Autofluorescence and diffuse reflectance spectroscopy and spectral imaging for breast surgical margin analysis," *Lasers Surg. Med.* **42**(1), 15–23 (2010).
24. M. A. Mastanduno et al., "Sensitivity of MRI-guided near-infrared spectroscopy clinical breast exam data and its impact on diagnostic performance," *Biomed. Opt. Express* **5**(9), 3103–3115 (2014).
25. A. N. Bashkatov et al., "Optical properties of human skin, subcutaneous and mucous tissues in the wavelength range from 400 to 2000 nm," *J. Phys. D: Appl. Phys.* **38**(15), 2543–2555 (2005).
26. N. Rajaram, T. H. Nguyen, and J. W. Tunnell, "Lookup table-based inverse model for determining optical properties of turbid media," *J. Biomed. Opt.* **13**(5), 050501 (2008).
27. B. S. Nichols, N. Rajaram, and J. W. Tunnell, "Performance of a lookup table-based approach for measuring tissue optical properties with diffuse optical spectroscopy," *J. Biomed. Opt.* **17**(5), 057001 (2012).
28. R. Michels, F. Foschum, and A. Kienle, "Optical properties of fat emulsions," *Opt. Express* **16**(8), 5907–5925 (2008).
29. C. Mätzler, "MATLAB functions for Mie scattering and absorption," Institut für Angewandte Physik, Bern, 2002, http://arrc.ou.edu/~rockee/NRA_2007_website/Mie-scattering-Matlab.pdf (22 October 2014).
30. D. Yudovsky and L. Pilon, "Retrieving skin properties from in vivo spectral reflectance measurements," *J. Biophotonics* **4**(5), 305–314 (2011).

31. S. L. Jacques, "Optical properties of biological tissues: a review," *Phys. Med. Biol.* **58**(11), R37 (2013).
32. D. Segelstein, "The complex refractive index of water," Master's Thesis, University of Missouri (1981).
33. R. L. P. van Veen et al., "Determination of VIS-NIR absorption coefficients of mammalian fat using time- and spatially resolved diffuse reflectance and transmission spectroscopy," *J. Biomed. Opt.* **10**(5), 054004 (2005).
34. R. Nachabé et al., "Estimation of lipid and water concentrations in scattering media with diffuse optical spectroscopy from 900 to 1600 nm," *J. Biomed. Opt.* **15**(3), 037015 (2010).
35. S. Prahl, "Tabulated molar extinction coefficient for hemoglobin in water," Oregon Medical Laser Center, 1998, http://omlc.ogi.edu/spectra/hemoglobin/summary.html (22 October 2014).
36. P. Crippa, V. Cristofoletti, and N. Romeo, "A band model for melanin deducted from optical absorption and photoconductivity experiments," *Biochim. Biophys. Acta* **538**(1), 164–170 (1978).
37. T. Sarna and R. Sealy, "Photoinduced oxygen consumption in melanin systems. Action spectra and quantum yields for eumelanin and synthetic melanin," *Photochem. Photobiol.* **39**(1), 69–74 (1984).
38. A. Kim and B. Wilson, "Measurement of ex vivo and in vivo tissue optical properties: methods and theories," in *Optical-Thermal Response of Laser-Irradiated Tissue*, A. J. Welch and M. J. C. Gemert, Eds., pp. 267–319, Springer, The Netherlands (2011).
39. B. C. Wilson and S. L. Jacques, "Optical reflectance and transmittance of tissues: principles and applications," *IEEE J. Quantum Electron.* **26**(12), 2186–2199 (1990).
40. T. Næs et al., *A User Friendly Guide to Multivariate Calibration and Classification*, NIR Publications, Chichester (2002).
41. P. Pudil, J. Novovicova, and J. Kittler, "Floating search methods in feature selection," *Pattern Recognit. Lett.* **15**(11), 1119–1125 (1994).
42. R. V. Bardale et al., "Evaluation of histologic changes of the skin in postmortem period," *Am. J. Forensic Med. Pathol.* **33**(4), 357–361 (2012).
43. H. Q. Woodard and D. R. White, "The composition of body tissues," *Br. J. Radiol.* **59**(708), 1209–1218 (1986).
44. V. A. Dubinskaya et al., "Comparative study of the state of water in various human tissues," *Bull. Exp. Biol. Med.* **144**(3), 294–297 (2007).
45. R. R. Warner, M. C. Myers, and D. A. Taylor, "Electron probe analysis of human skin: determination of the water concentration profile," *J. Invest. Dermatol.* **90**(2), 218–224 (1988).
46. P. Meredith and T. Sarna, "The physical and chemical properties of eumelanin," *Pigm. Cell Res.* **19**(6), 572–594 (2006).
47. K. Watts et al., "Melanin content of hamster tissues, human tissues, and various melanomas," *Cancer Res.* **41**(2), 467–472 (1981).
48. M. Rins et al., "Skin density in the hairless rat. Evidence of regional differences," *Eur. J. Drug Metab. Pharmacokinet.* **3**, 456–457 (1991).
49. S. G. Coelho et al., "Non-invasive diffuse reflectance measurements of cutaneous melanin content can predict human sensitivity to ultraviolet radiation," *Exp. Dermatol.* **22**(4), 266–271 (2013).
50. R. M. P. Doornbos et al., "The determination of in vivo human tissue optical properties and absolute chromophore concentrations using spatially resolved steady-state diffuse reflectance spectroscopy," *Phys. Med. Biol.* **44**(4), 967–981 (1999).
51. S.-H. Tseng et al., "Chromophore concentrations, absorption and scattering properties of human skin in-vivo," *Opt. Express* **17**(17), 14599–14617 (2009).
52. J. C. Graham and R. K. Myers, "The prognostic significance of angiogenesis in canine mammary tumors," *J. Vet. Intern. Med.* **13**(5), 416–418 (1999).
53. B. Rong-jie et al., "Solitary pulmonary nodules: comparison of multislice computed tomography perfusion study with vascular endothelial growth factor and microvessel density," *Chin. Med. J.* **122**(5), 541–547 (2009).
54. M. I. Carvalho et al., "EGFR and microvessel density in canine malignant mammary tumours," *Res. Vet. Sci.* **95**(3), 1094–1099 (2013).
55. J. Eurell and D. van Sickle, "Connective and supportive tissue," in *Textbook of Veterinary Histology*, H. Dellmann and J. Eurell, Eds., 5th ed., pp. 32–61, Williams & Wilkins, Baltimore, Maryland (1998).
56. R. Nachabe et al., "Diagnosis of breast cancer using diffuse optical spectroscopy from 500 to 1600 nm: comparison of classification methods," *J. Biomed. Opt.* **16**(8), 087010 (2011).

Blaž Cugmas is a postdoctoral researcher in Sensum and an associate member of the Laboratory of Imaging Technologies. His research interests involve the processing of biomedical signals and the analysis of tissues with diffuse reflectance spectroscopy.

Tanja Plavec is an assistant professor at the Clinic for Small Animal Medicine and Surgery, University of Ljubljana. She works in the Surgery Department of the clinic, and her interests concentrate on oncological and soft tissue surgeries.

Maksimilijan Bregar is a PhD student in the Department of Electrical Engineering, University of Ljubljana. He is a member of the Laboratory of Imaging Technologies, and his research interests focus on contact pressure-aided spectroscopy and experimental techniques for measuring tissue optical properties.

Peter Naglič is a PhD student in the Department of Electrical Engineering, University of Ljubljana. He is a member of the Laboratory of Imaging Technologies. His research interests involve computer modeling of light propagation in turbid media and experimental techniques for measuring their optical properties.

Franjo Pernuš is a professor in the Department of Electrical Engineering, University of Ljubljana. He is head of the Laboratory of Imaging Technologies, and his research interests involve biomedical image processing and analysis, computer vision, and the applications of image processing and analysis techniques to various biomedical and industrial problems. He is a cofounder of the high-tech company Sensum, which supplies machine vision solutions for the pharmaceutical industry.

Boštjan Likar is a professor in the Department of Electrical Engineering, University of Ljubljana. He is a member of the Laboratory of Imaging Technologies, and his research interests focus on visual quality inspection, computer and machine vision systems, biomedical image processing, and hyperspectral imaging. He is a cofounder of the high-tech company Sensum, which supplies machine vision solutions for the pharmaceutical industry.

Miran Bürmen is an assistant professor in the Department of Electrical Engineering, University of Ljubljana. He is a member of the Laboratory of Imaging Technologies, and his research interests concentrate on the development of hyperspectral imaging systems for various biomedical and industrial applications.